ENGINEERING DESIGN MEMO
(For Internal Use Only)

PROJECT: DCAT Validation	**TITLE**: **Finesse DCAT Validation using ASU Disk Cavity Rig**	**EDM00000**
ORIGINATOR: **Cloud Cheung**		**SECTION**:
DATE: Aug. 09, 2024	**REVISION**: 1	**PAGE**: 1

Summary

This report documents Finesse’s Disk Cavity Analysis Tool (DCAT) connector validation for the radial in-flow case. The Finesse model encompasses the exit towards to the hub, the preswirler, discourager (rim seal), and exit into the main stream flow without the presence of blades or vanes. The work is motivated by the lack of documentation specifically for radial in-flow cases, with the creator of the DCAT, Michael Okpara, explicitly mentioning that DCAT struggles with radial in-flow for both stator-rotor and rotor-rotor configurations. This study focuses on the stator-rotor configuration and seeks to validate the outputs provided by Finesse, against experimental data from the ASU Disk Cavity Research Rig (2005), as well as CFD. Results including preswirler tangential exit velocity (swirl) and static pressure are compared across all three methods for disk cavity analysis, and are compared for the documentation of best practices when operating in Finesse and to better understand how the DCAT performs for various flow rates.

The Arizona State University Disk Cavity Research Rig and Analysis Approach

The disk cavity within this project is modeled after the Arizona State University (ASU) Disk Cavity Research Rig and compared with the results of the data obtained by Dr. Ram Roy from Solar sponsored research between 2004-2005 (Refs. [1-2]). Figure 1 depicts the ASU disk cavity research rig, and Figure 2 shows the schematic detailing the flow path.

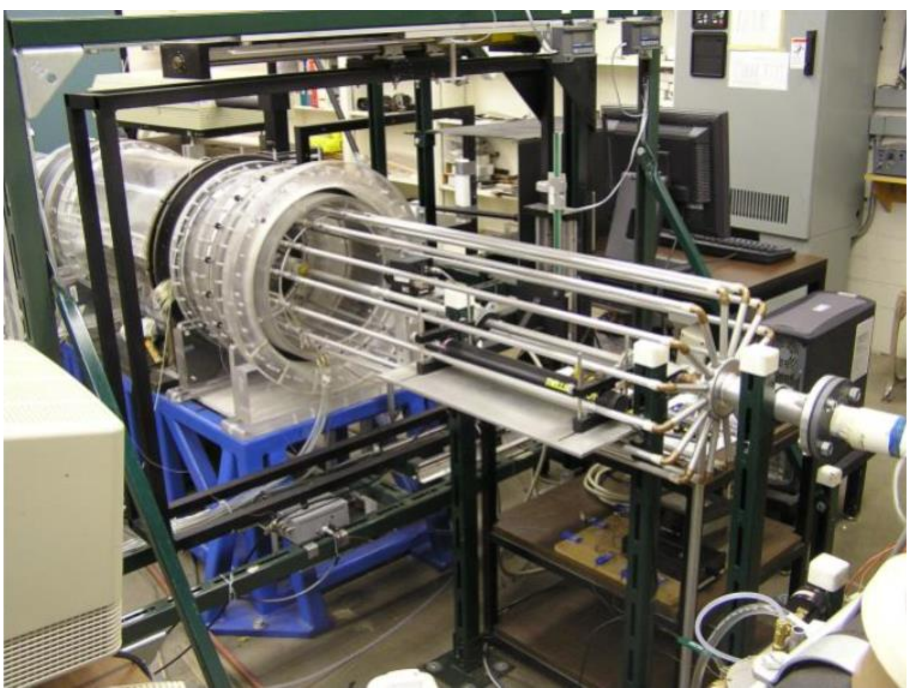

Figure 1 ASU disk cavity research rig

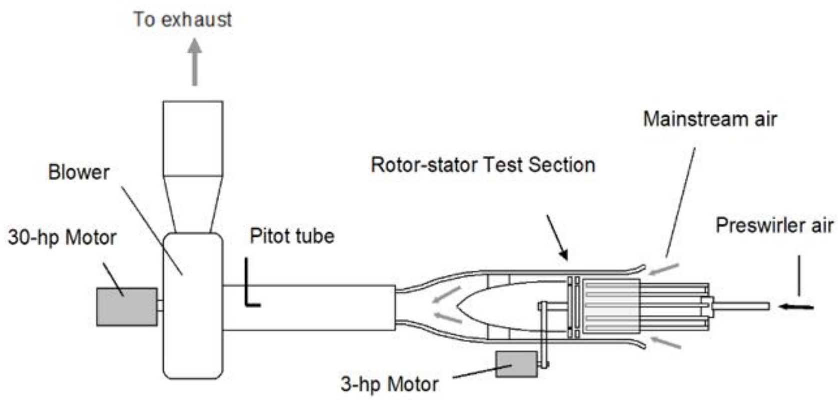

Figure 2 ASU disk cavity research rig schematic

The report in Ref. [1] details the geometry of the disk cavity, shown in Figure 3, and was used to recreate the model in Finesse. The report also provides the radially varying static pressure sampled from probes along the stator, as well as the outputs from predictions made by a standalone DCAT model. For these reasons, the ASU disk cavity rig was selected for a comprehensive DCAT validation. The report documents four sets of data, each containing three tests conducted at a low, intermediate, and high flow rate. The first two sets of data (containing results from six different flow rates) are simulated in Finesse, and later CFD, to compare the mass flow rates, static pressure, and swirl throughout the cavity.

ENGINEERING DESIGN MEMO
(For Internal Use Only)

PROJECT: DCAT Validation	**TITLE**: **Finesse DCAT Validation using ASU Disk Cavity Rig**	**EDM00000**
ORIGINATOR: **Cloud Cheung**		**SECTION**:
DATE: Aug. 09, 2024	**REVISION**: 1	**PAGE**: 3

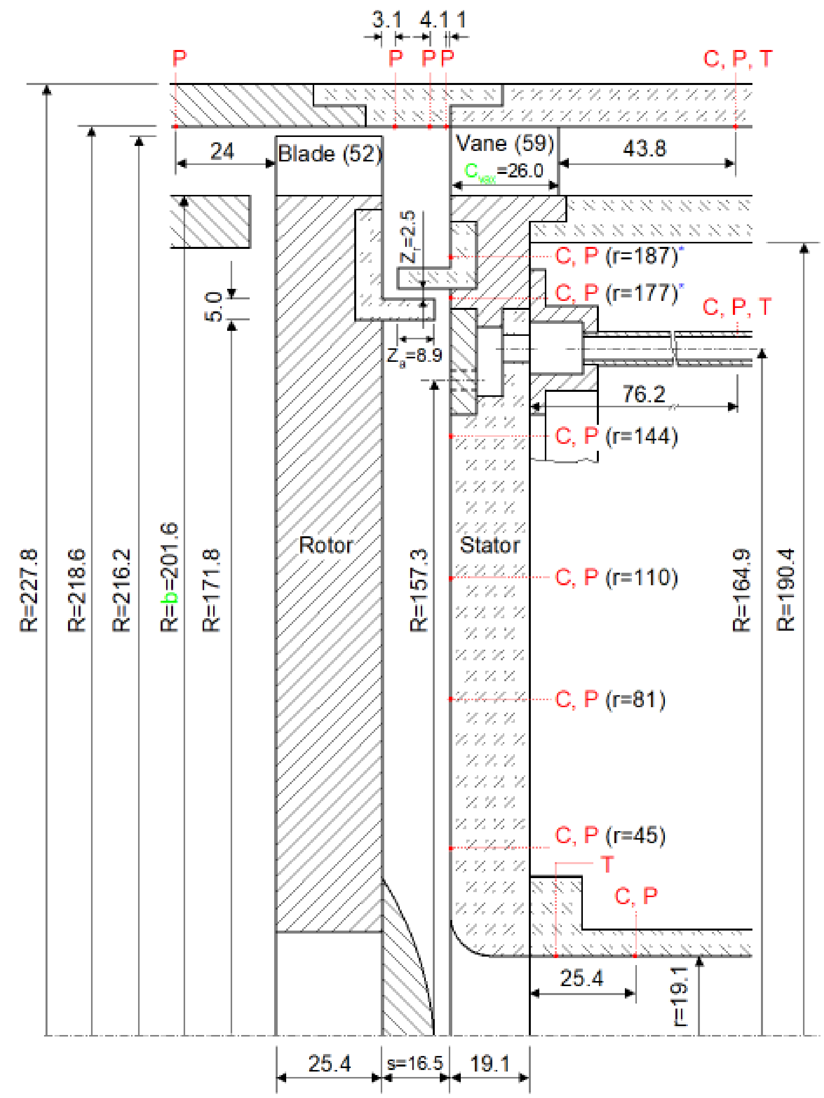

* Circumferentially 5 locations over one vane pitch

All dimensions in mm

Figure 3 Diagram of the disk cavity geometry and locations for pressure probes

Modeling in Finesse and Mass Flow Balancing

The Finesse model of the ASU disk cavity research rig is shown below in Figure 4, and it models the geometry between 28.7 mm < r < 187 mm, which captures the hub bend to the discourager. The discourager and hub bend are both modeled as standard orifices that capture the annular geometry of the rig. The preswirler is modeled as a preswirler orifice with a multiplicity of 30 as the rig uses a preswirler ring with 30 discreet drilled holes. Lastly, the DCAT connector models the region directly below the discourager and connects to the same node as the preswirler. DCAT outputs have been documented in Appendix A for more information regarding the exact inputs.

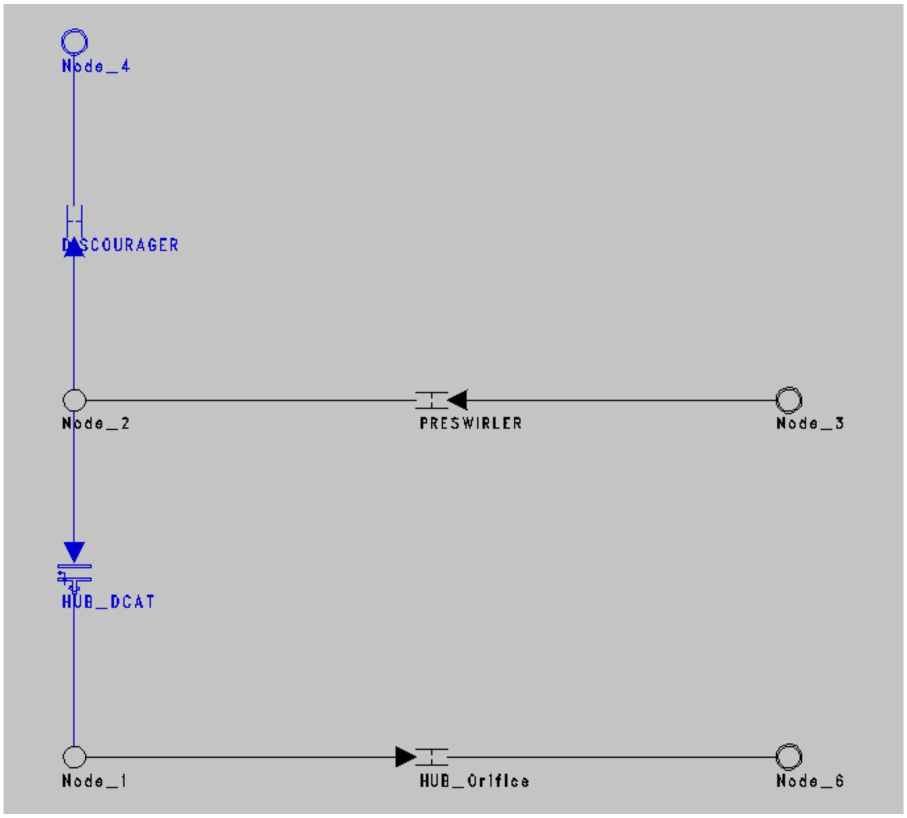

Figure 4 Finesse model of the ASU disk cavity research rig

As a new user, assembling the model in Finesse proved challenging. So to obtain a converging model with mass flow that matched the rig within each branch, a solving method was a necessity. One such method is described below in Figure 5, and utilizes Finesse's built in flow optimization solver. Adjusting the discharge coefficients allow the user to fine-tune the orifices—which act as flow metering devices for the DCAT—and eventually balance the flow rate within the model.

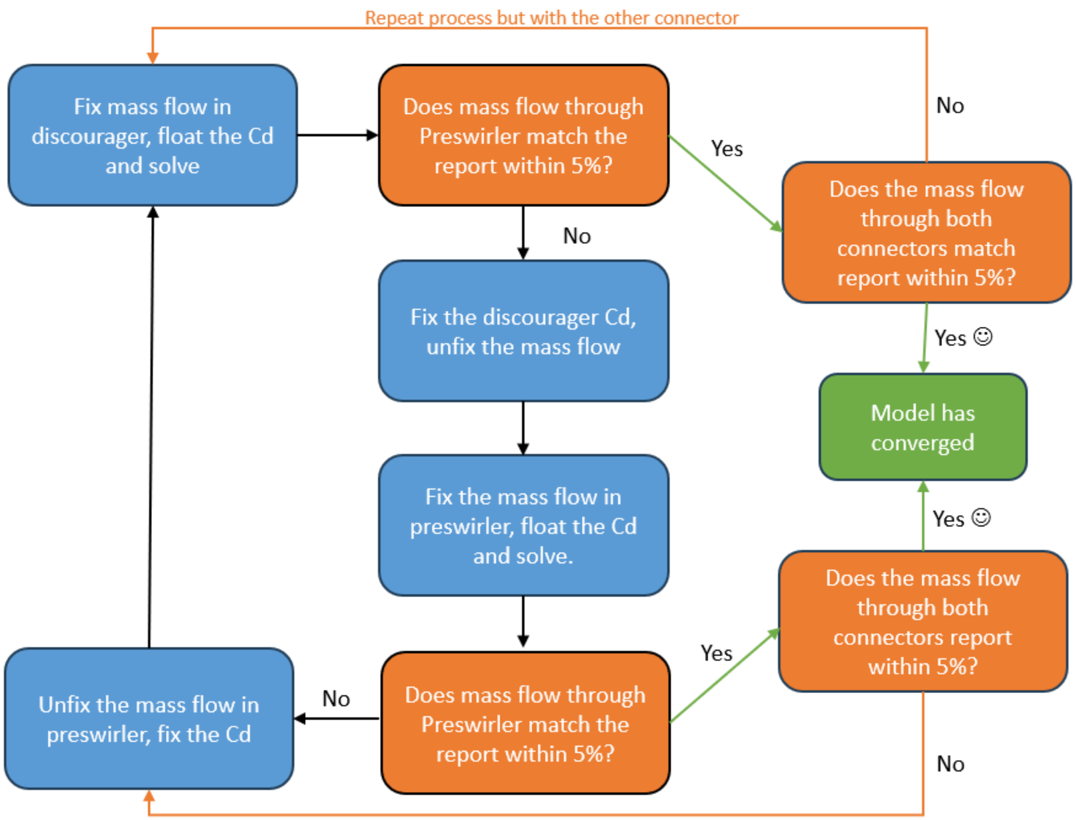

Figure 5 Flowchart describing the mass balancing processes for the Finesse model

Another method for trouble shooting unconverging mass flows is to isolate and adjust specific components. One such case is the preswirler. Adjusting the preswirler was a critical step in the process as the preswirler definition greatly affects the overall flow and swirl within the cavity. An isolated preswirler model shown in Figure 6 may be solved repeatedly across different pressure ratios to generate a curve describing the mass flow through the connector as shown in Figure 7a. It is apparent that the default preswirler overpredicts the mass flow. To remedy this, the discharge coefficient is manually solved for by setting the pressure ratio and target mass flow in the model as defined by the report. Unfixing the discharge coefficient will allow for it to be solved using optimized flow imbalance, and the same process above can be used to generate the curve from Figure 7b to show the agreement between the mass flow of the adjusted preswirler and that from the report. For this project, a discharge coefficient and preswirler effectiveness was computed for each of the three flow rates and then averaged to produce a single value used in the final system.

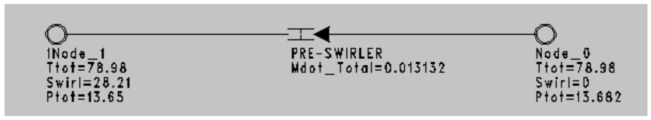

Figure 6 Isolated preswirler model for fine-tuning

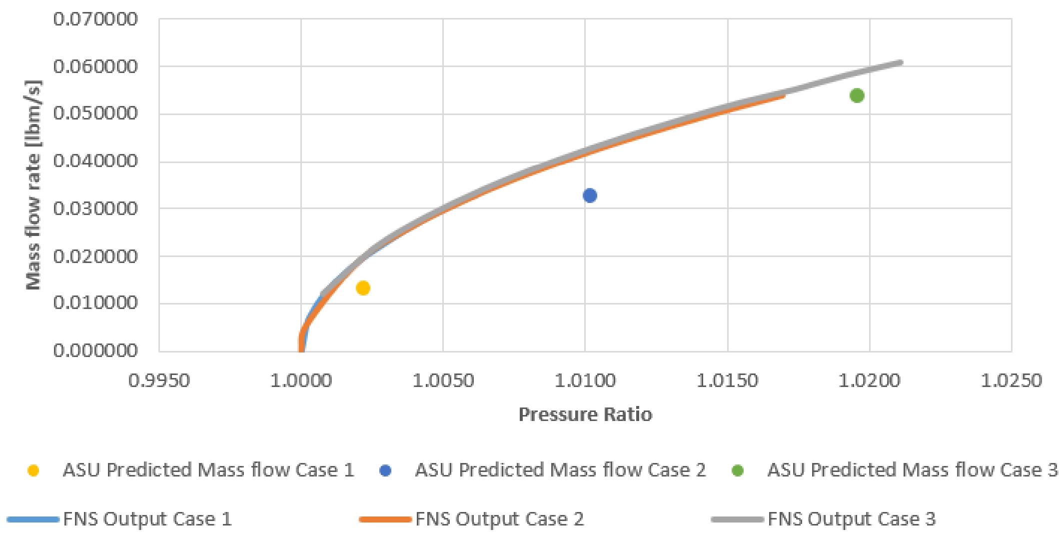

(a) Mass flow through the unadjusted preswirler

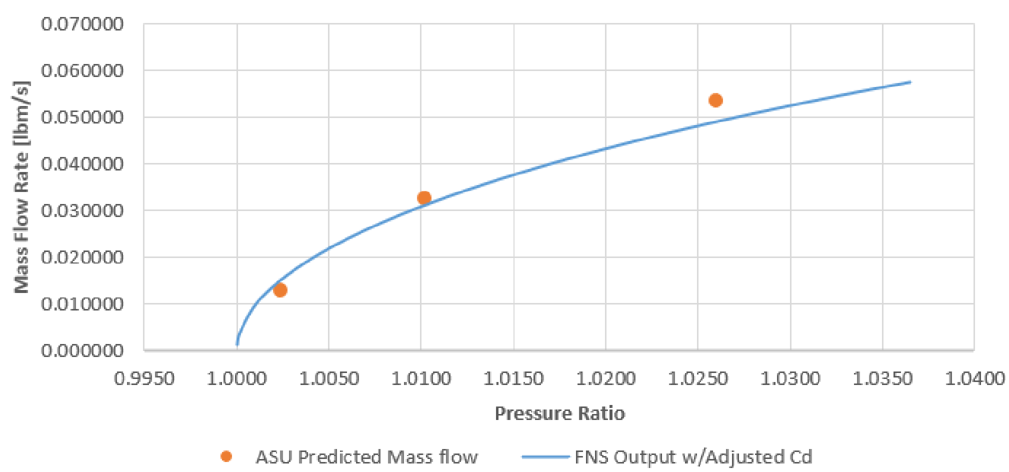

(b) Mass flow through the adjusted preswirler

Figure 7 Preswirler mass flow rate agreement with ASU measured flow rates

After implementing the preswirler adjustments and completing the mass balancing process for the Finesse model from Figure 4, the static pressure across the DCAT connector is compared to the data provided by the ASU report. Figure 8b and 8c showcases the disagreement between the Finesse results and those reported by ASU, with Finesse greatly overpredicting the static pressure across the disk cavity for the two cases of higher flow rates. At the lower flow rate setting, the Finesse model continues to have difficulty with converging mass flow and it is shown in the strange curve produced by both the stand alone DCAT from the report, as well as from the stagnant pressures produced by the current DCAT in Finesse in Figure 8a.

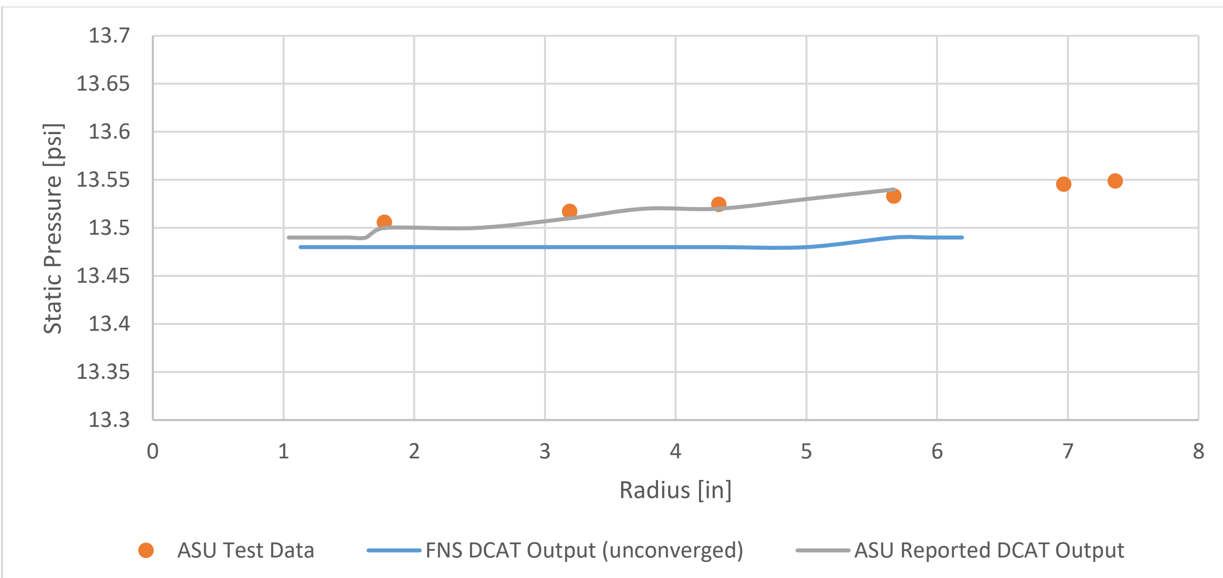

(a) $c_w = 1923$

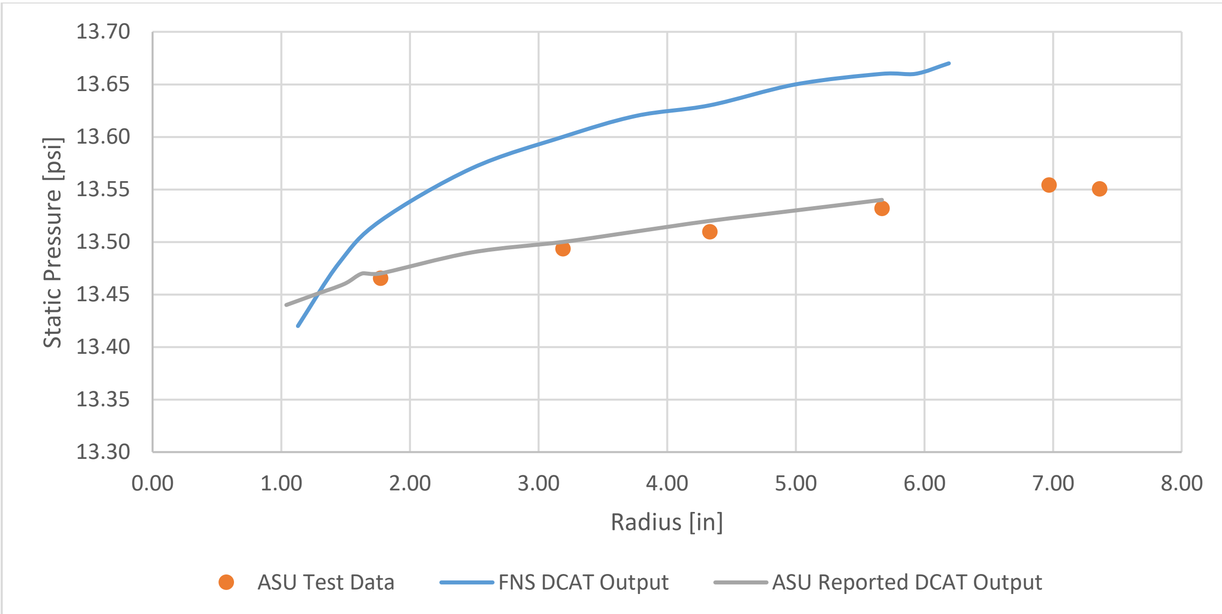

(b) $c_w = 4806$

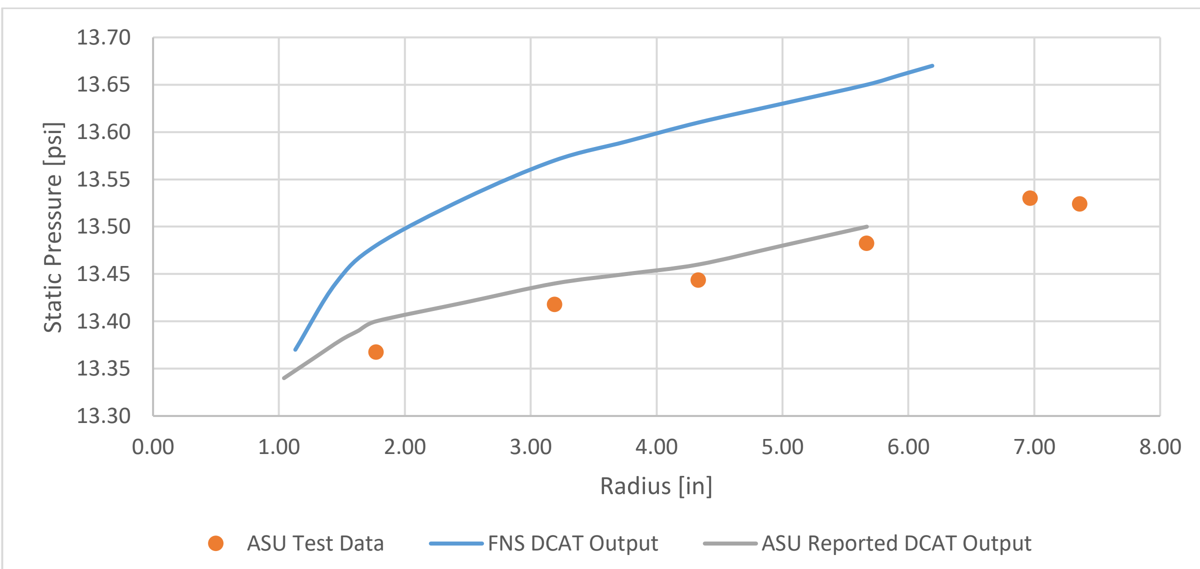

(c) $c_w = 7370$

Figure 8 Initial plots of the radially varying static pressure between ASU Data, standalone DCAT, and FNS DCAT for three different flow rates

It is assumed that there must be a bug or mistake within the Finesse model as these results are not enough to suspect the DCAT as the primary source of error in the study. From previous reports, it is known that Finesse and CFD tend to have good agreement. A logical next step is run this disk cavity using CFD to gain insight on why the Finesse model is not meeting expectations.

CFD Modeling and Results

The study employed STAR-CCM+ v. 18.06 for all flow simulations and used the built-in CAD modeler to design and construct the geometry, based on the schematic from Figure 3. The approach for the CFD study is much like other standard practices, following a series of mesh refinements and sensitivity studies before conducting the simulations and presenting results. STAR is a complex program, and the following studies would not be possible without the tutorials created by Hans Hamm.

The geometry is shown below in Figure 9 and as an example of the inputs, the boundary conditions for Set II: $c_w = 7370$ are shown in Figure 10. The preswirler is a simple circular cylinder extruded tangentially from the cavity at an angle of 10° into a preswirler chamber where the purge conditions are later defined.

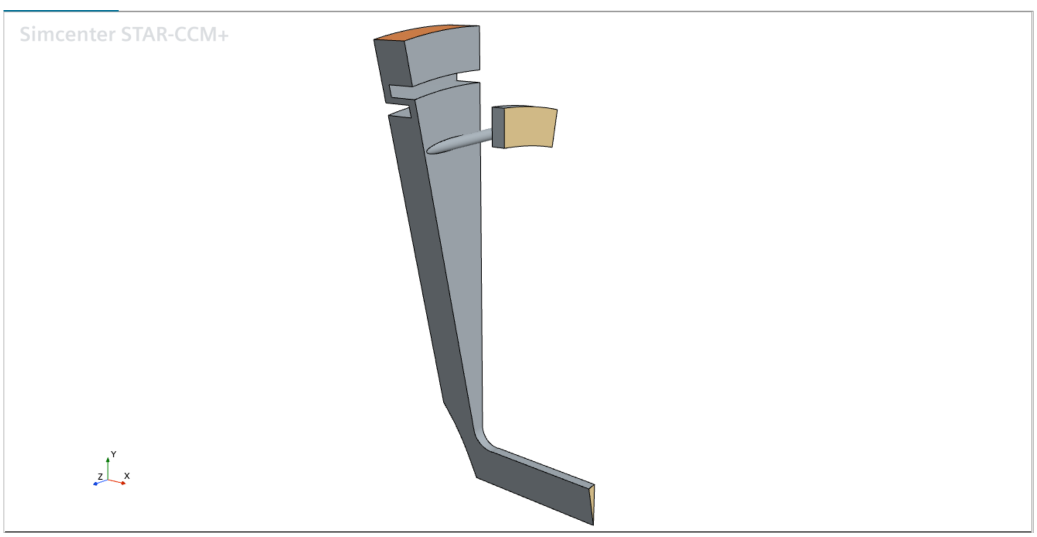

Figure 9 The disk cavity geometry as created in the STAR-CCM+ CAD modeler

Boundary conditions for each test are documented in Appendix C, however Figure 10 shows a sample of the conditions used for a simulation of the Set II: $c_w = 7370$ test conditions. The surface where flow exits to the mainstream is modeled as a pressure outlet and the purge wall and hub wall are modeled as mass flow inlet. The hub flow rate is negative to model the flow exiting the cavity. Both mass inlets utilize a 1/30th of the total reported mass flow as the model is periodic, and only 12-degree sector. Temperature is also defined at each inlet and outlet according to the ASU report.

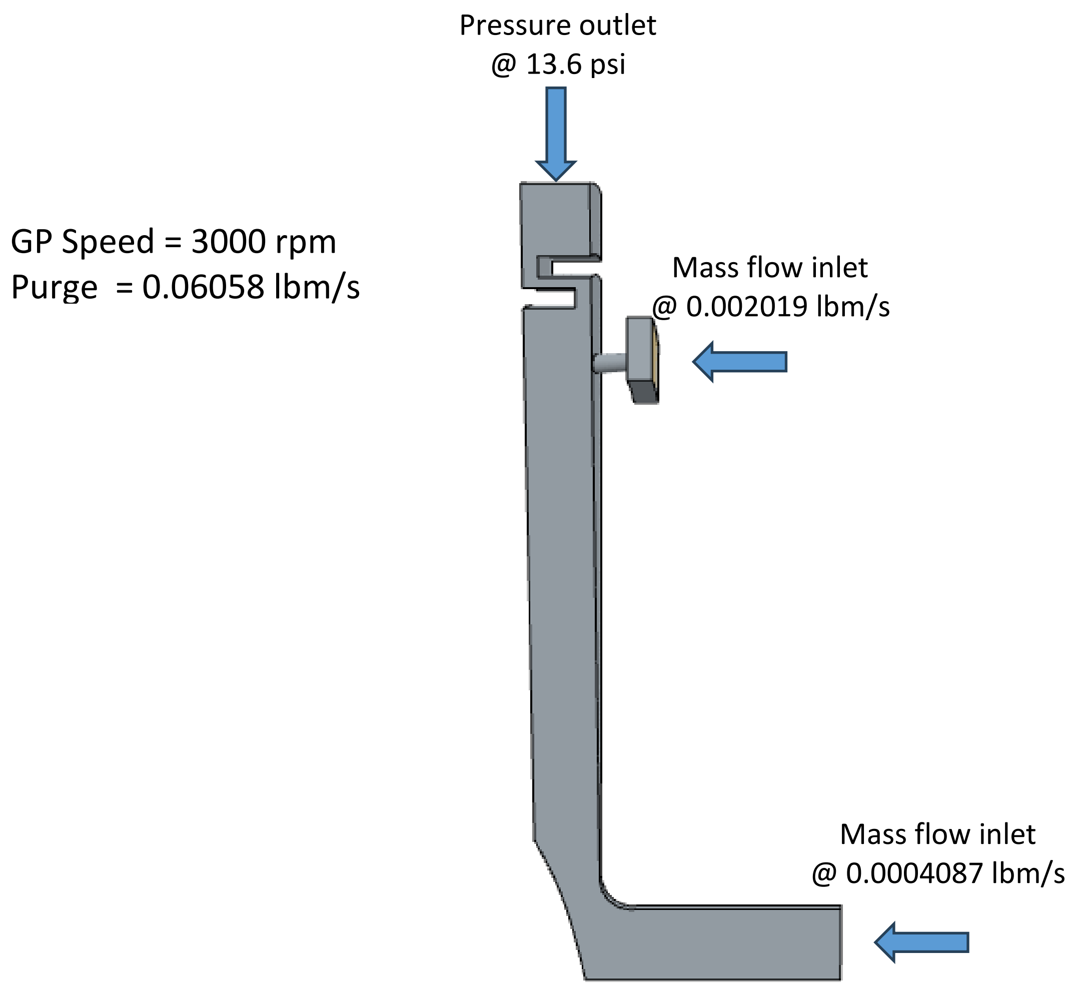

Figure 10 Sample boundary conditions inputs using data from Set II: $c_w = 7370$ **(Ref. [1])**

Mesh Sizing

Table 1 Mesh Custom Controls

	Target Surface Size	Num. Prism Layers	Min. Surface Size
Discourager	50%	12	10%
Inner Walls	20%	16	10%
No Prism	100%	-	10%
Preswirler Walls	33.33%	12	10%

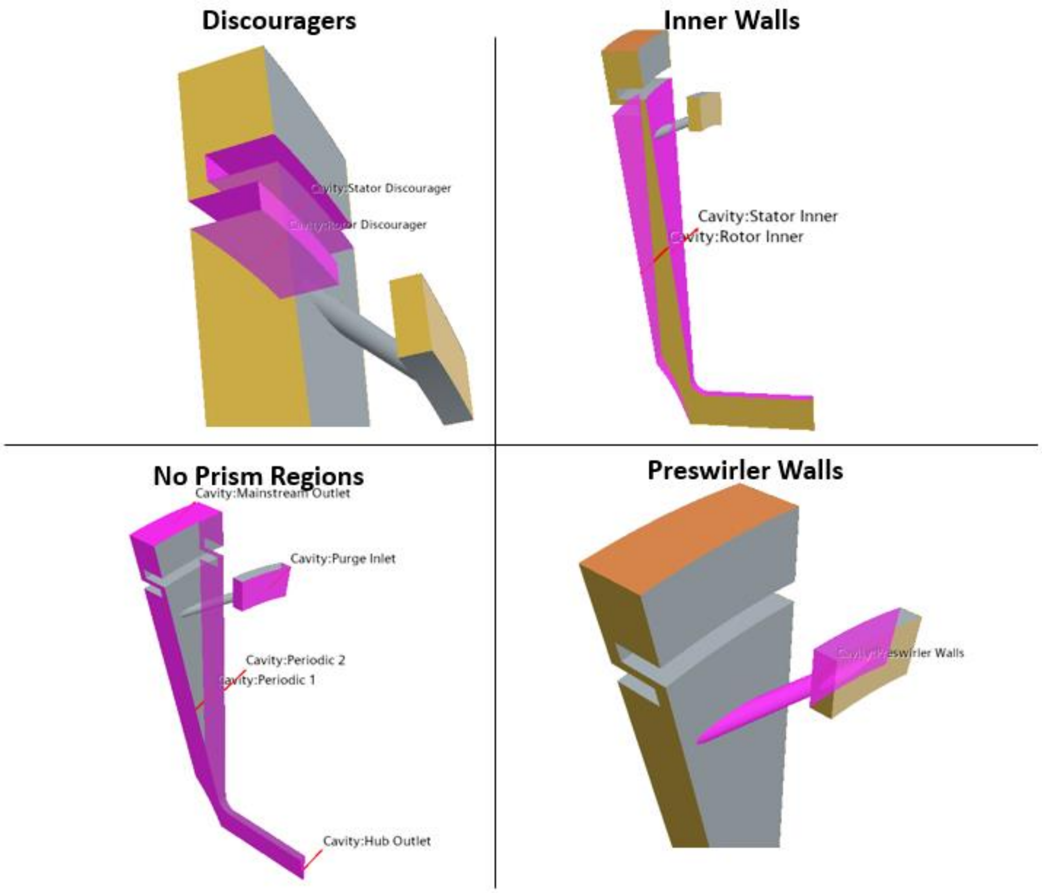

Figure 11 Surfaces using custom mesh controls

Mesh Sensitivity Study

As a best practice, a mesh sensitivity study was conducted to detect mesh dependencies for the model. A cylindrical volume between 144 mm < r < 187 mm was refined under five different settings shown in Figure 12, with the results of the study being shown in Figure 13. The differences in static pressure across the disk cavity was below 0.1% across all cases. Therefore, the original mesh settings were selected to minimize the computational power required to simulate the model.

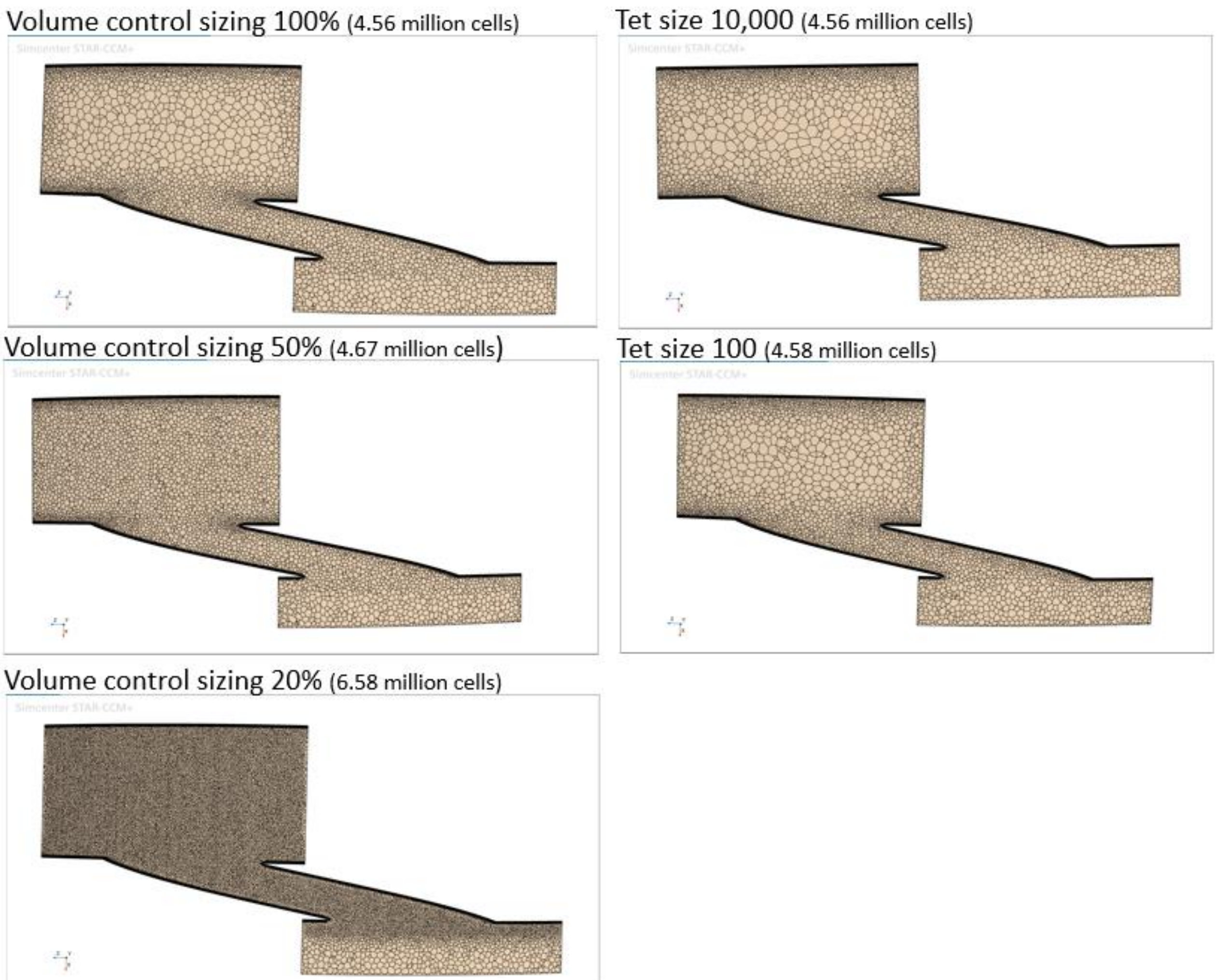

Figure 12 Cross section of the volume control region showing the cell sizing differences between the five tested mesh settings

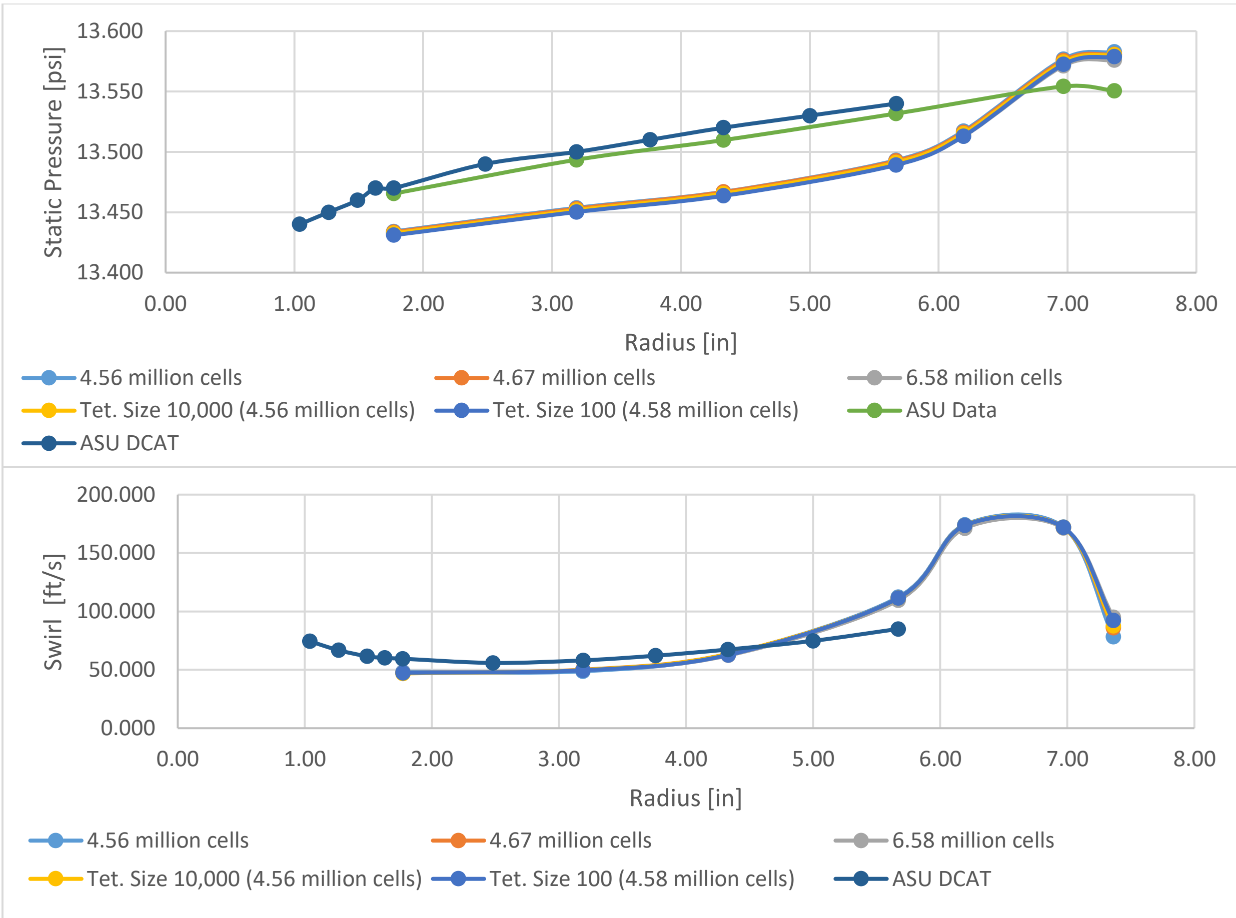

Figure 13 Mesh sensitivity study results for static pressure (top) and swirl (bottom)

CFD Results

Steady state solutions obtained are shown below in Figure 14 which describes the absolute pressure along the cavity in a static graphic. Rotating cavity flow is difficult to fully encapsulate in images, however the original model and animations have been archived. Snapshots of the cross section of the mid plane and preswirler plane are provided in Figures 15 and 16, respectively.

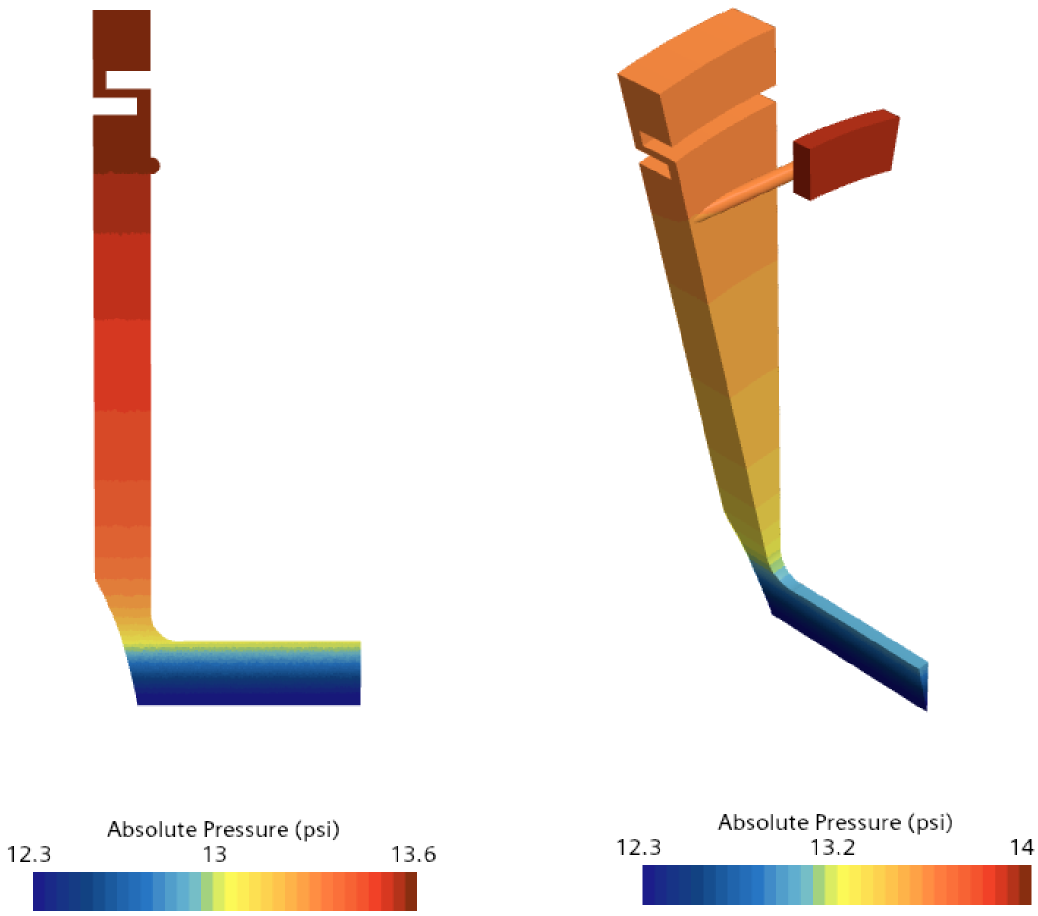

Figure 14 Absolute pressure along the midplane (left) and contour (right)

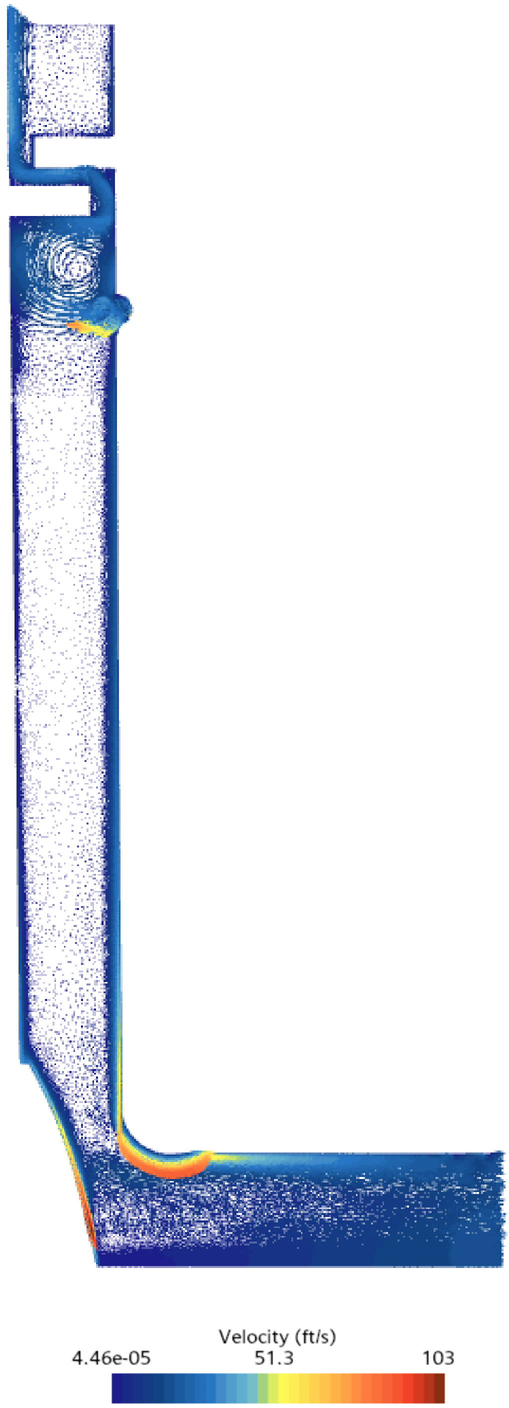

Figure 15 Tangential projection of velocity from a lab frame of reference

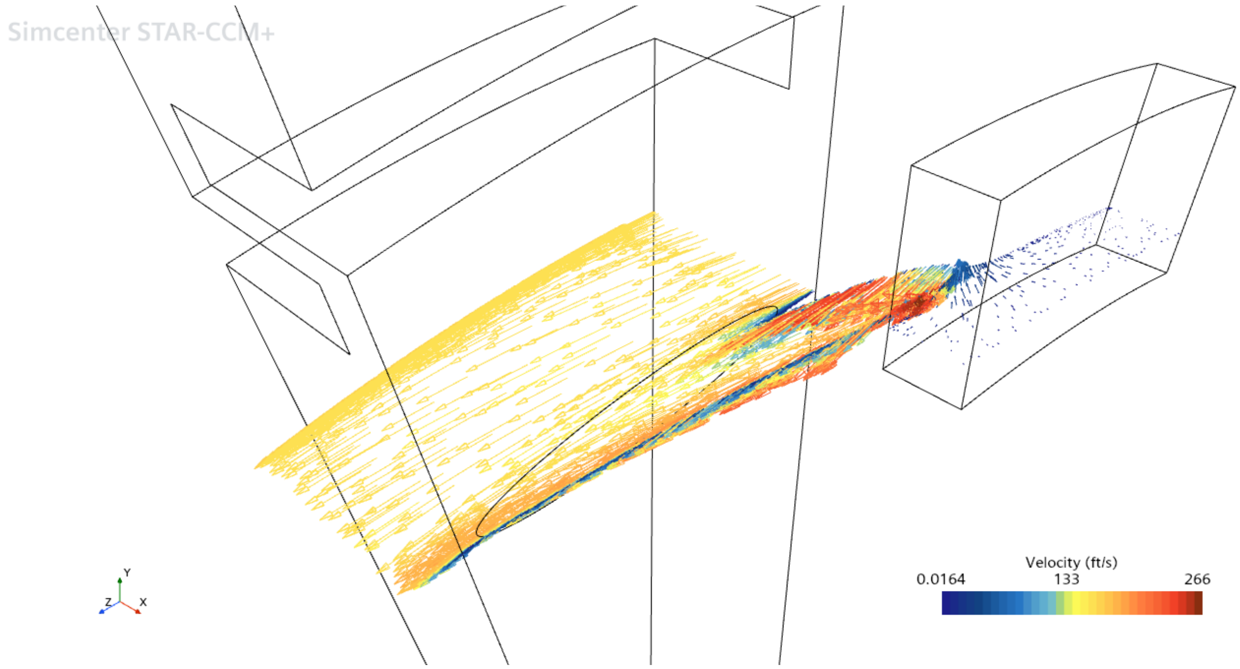

Figure 16 Lab frame velocity at the cavity cross-section at the preswirler inlet

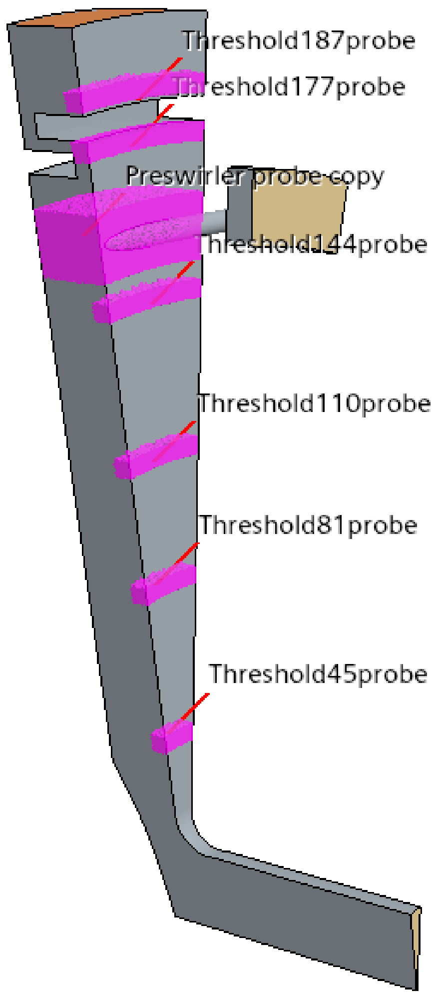

Figure 17 All probe locations for collecting CFD report values

Table 2 Static pressure and swirl for Set I results from CFD

		Set I: $c_w = 1602$		**Set I:** $c_w = 4005$		**Set I:** $c_w = 6569$	
Radius [mm]	Radius [in]	Ps [psi]	Swirl [ft/s]	Ps [psi]	Swirl [ft/s]	Ps [psi]	Swirl [ft/s]
45.00	1.77	13.70	39.75	13.43	70.53	13.42	105.03
81.00	3.19	13.71	38.03	13.47	59.61	13.49	84.35
110.00	4.33	13.72	41.34	13.49	64.14	13.53	89.45
144.00	5.67	13.73	46.42	13.51	85.86	13.57	129.15
157.30	6.19	13.73	52.21	13.52	80.78	13.59	130.37
177.00	6.97	13.74	82.41	13.53	81.64	13.61	111.80
187.00	7.36	13.74	54.48	13.53	51.53	13.61	67.92

Table 3 Static pressure and swirl for Set II results from CFD

		Set II: $c_w = 1923$		**Set II:** $c_w = 4806$		**Set II:** $c_w = 7670$	
Radius [mm]	Radius [in]	Ps [psi]	Swirl [ft/s]	Ps [psi]	Swirl [ft/s]	Ps [psi]	Swirl [ft/s]
45.00	1.77	13.57	44.19	13.45	85.73	13.33	123.41
81.00	3.19	13.59	43.4	13.50	71.44	13.43	98.54
110.00	4.33	13.6	48.36	13.53	76.36	13.48	103.75
144.00	5.67	13.61	53.89	13.56	103.06	13.53	147.67
157.30	6.19	13.61	59.48	13.57	96.97	13.56	147.93
177.00	6.97	13.62	92.48	13.58	95.79	13.59	127.43
187.00	7.36	13.62	62.13	13.58	60.52	13.59	78.10

Final Comparisons between FNS, CFD, and Data

After completing the simulations on STAR, I revisited Finesse to troubleshoot and use new insights gained from the CFD to fix the model. It has been previously well documented that Finesse and CFD have good agreement, so a method to check the validity of the Finesse model is to use the CFD outputs as new inputs and see if there is agreement between the output of Finesse. These results are plotted in Figure 18 below. Immediately, good agreement between Finesse and CFD is apparent, and the primary difference is that the pressure at the hub probe location reported by the CFD was 1.7% lower than measured by ASU. Thus it is demonstrated that Finesse has a small window for variation in pressure for the hub input that will have a great effect on the overall development of the pressure distribution in the cavity. With this in mind, we may adjust the other models' inputs in a similar fashion and finally produce the results that are documented in Figure 19 and 20.

ENGINEERING DESIGN MEMO
(For Internal Use Only)

PROJECT: DCAT Validation	**TITLE**: **Finesse DCAT Validation using ASU Disk Cavity Rig**	**EDM00000**
ORIGINATOR: **Cloud Cheung**		**SECTION**:
DATE: Aug. 09, 2024	**REVISION**: 1	**PAGE**: 20

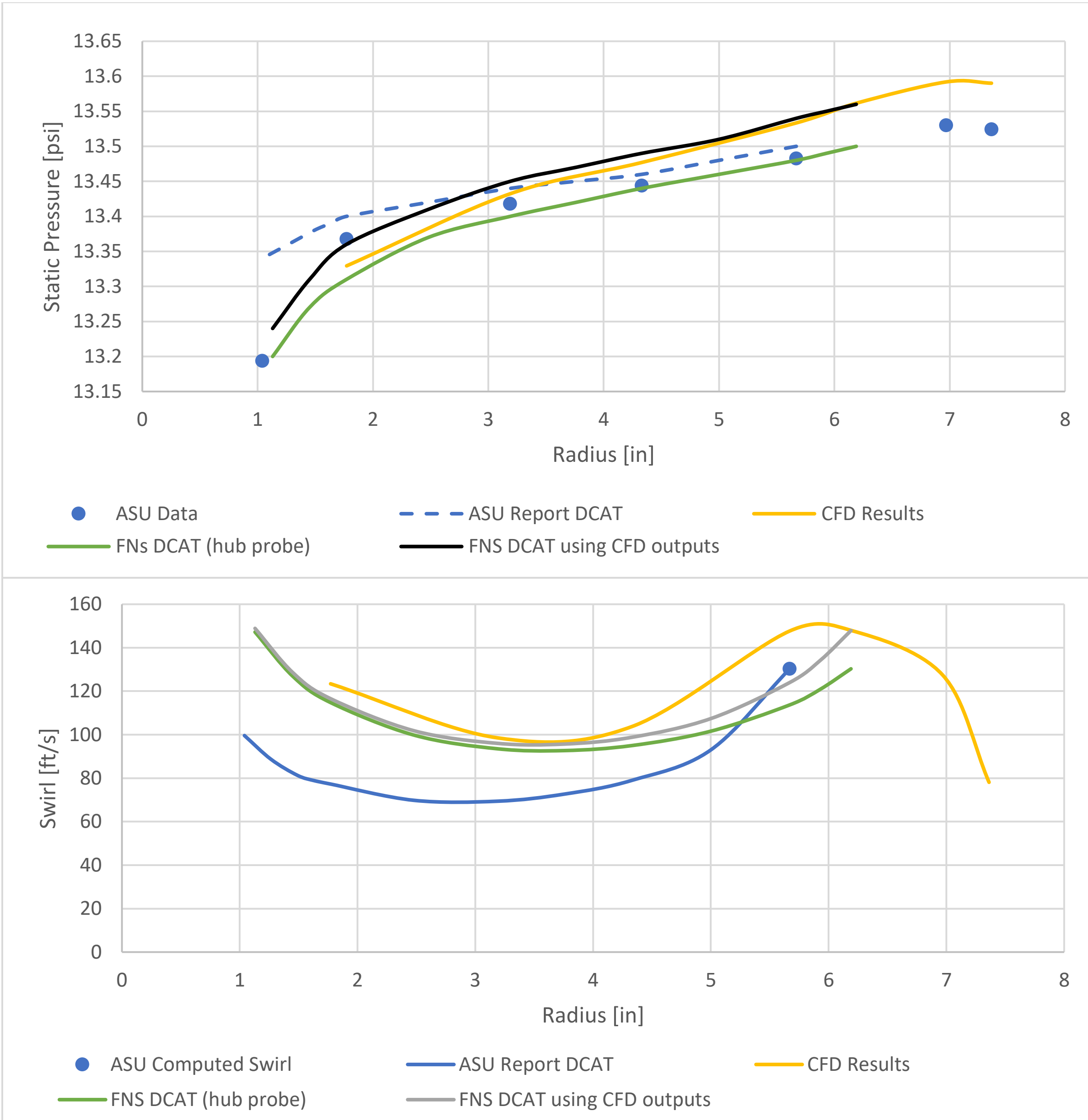

Figure 18 FNS results when the CFD outputs are applied as new inputs demonstrating the expected agreement between the two codes

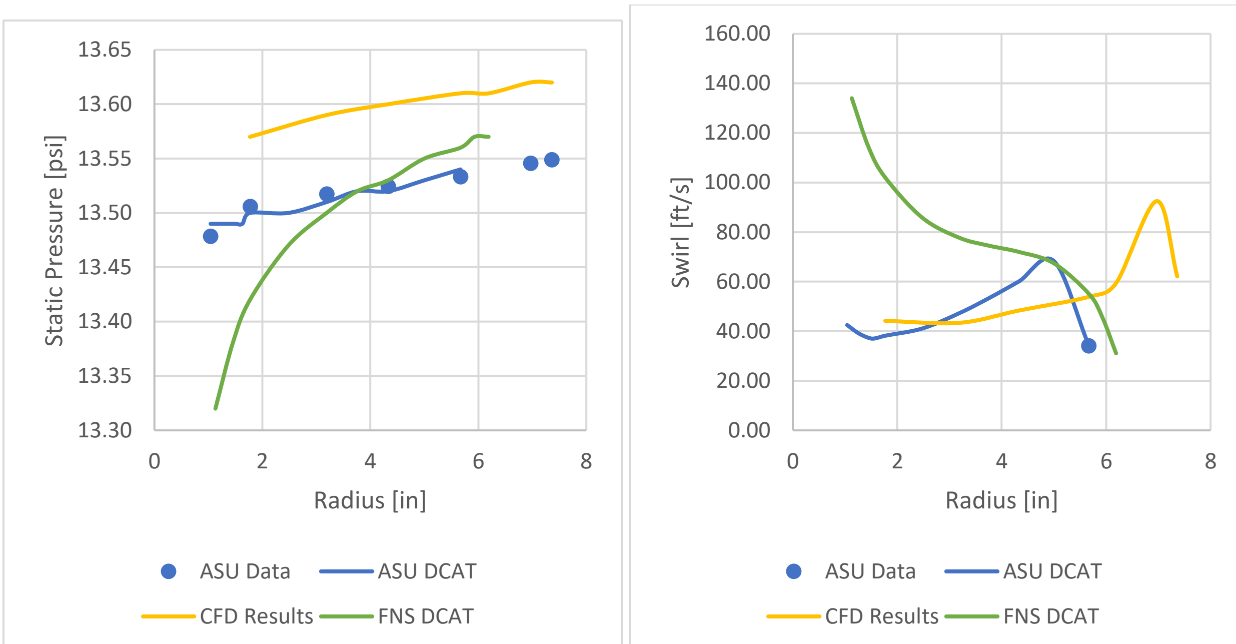

(a) Set II: $c_w = 1923$

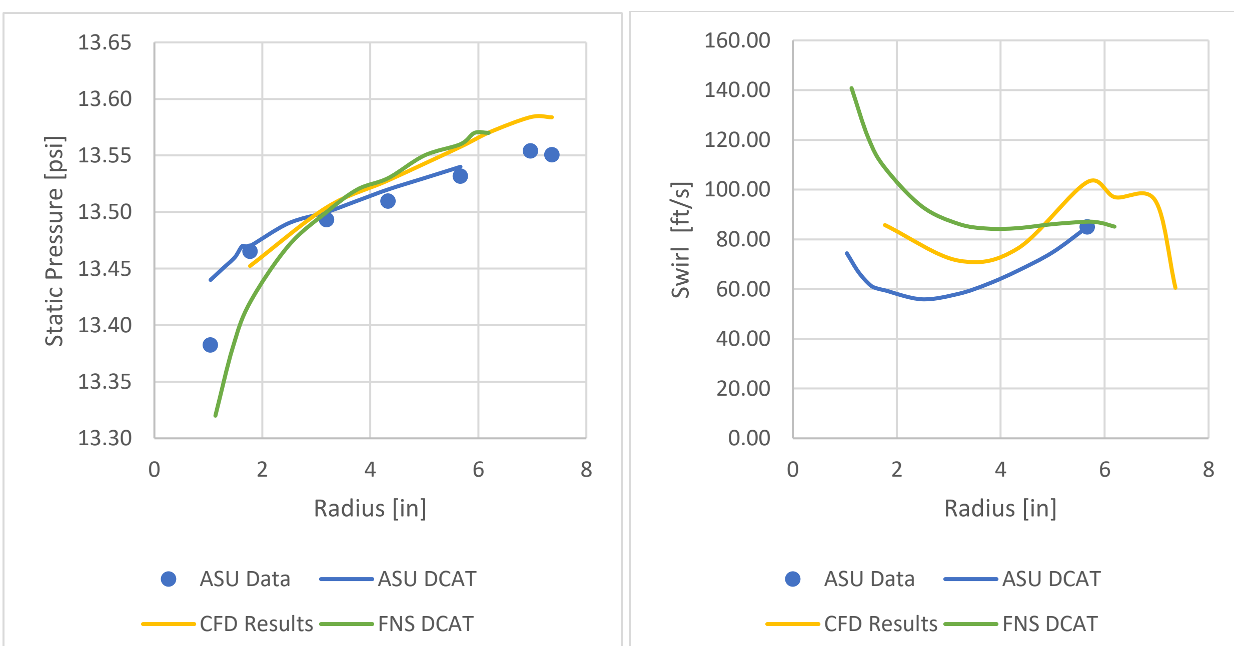

(b) Set II: $c_w = 4806$

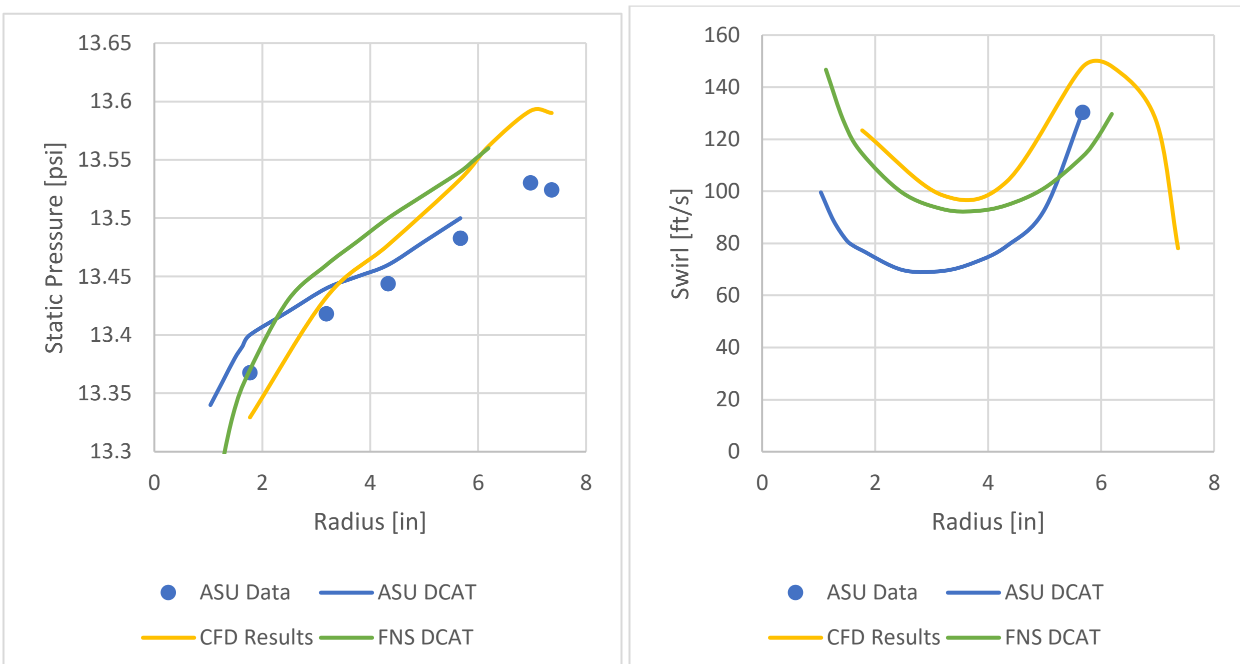

(c) Set II: $c_w = 7370$

Figure 19 Static pressure and swirl distributions along the cavity for Set II conditions

The second and third set of plots show a good match between the CFD, FNS, and data, however we see inaccuracies in the most radially inboard region of the cavity for both pressure and swirl. For the second flow rate at $c_w = 4806$, we note that radially inward, the Finesse DCAT tends to under predict pressure, but greatly overpredict swirl. Radially outboard, we see over prediction in pressure, but a good match in swirl. In the high flow rate case, we see similar trends in the curve which demonstrate decent agreement, however there is much more over prediction across the cavity for pressure but more agreement near the hub. The swirl curve matches better as well but experiences a large amount of over prediction.

For Figure 19a, we still see much disagreement between both programs and the data. The disagreement between CFD and the data needs to be further investigated, and the Finesse model did not have a converging mass flow. The DCAT seems to struggle with passing such small mass flows despite adjustment to the relaxation factor and this is a point for future studies.

Conclusions

- Uncertainty in the ASU reported pressures and lack of information near the preswirler makes it difficult to accurately model.
- Low flow cases need to be investigated more to understand underlying issues regarding convergence and mass flow.
- FNS's DCAT connector tends to under predict static pressure at radially inboard locations, and over predict at radially outboard locations.
- FNS's DCAT connector generally is over predicting swirl radially inboard of the preswirler.

References

1. Y. Kim, "ASU Disk Cavity Research – Results summary Part I: Pressure & cooling effectiveness", EDM0103
2. Y. Kim, "ASU Disk Cavity Research – Progress Report", EDM0087

Appendix A

DCAT_Calibration_Set1_Test1_20240701.fni (unconverged)

Rad	Gap	Trel	Tmetd	Tawd	Tt	Taws	Tmets	Ps
6.19	0.65	78.2	82	78.1	78.1	78	82	13.56
5.93	0.65	78.1	82	78	78.1	78.1	82	13.55
5.67	0.65	78	82	77.9	78.1	78.1	82	13.55
5	0.65	77.7	82	77.7	78.1	78.1	82	13.54
4.33	0.65	77.5	82	77.5	78.1	78.1	82	13.52
3.76	0.65	77.4	82	77.4	78.1	78.1	82	13.51
3.19	0.65	77.2	82	77.2	78.1	78	82	13.48
2.48	0.65	77.1	82	77.1	78.1	78	82	13.42
1.77	0.65	77.1	82	76.9	78.1	77.8	82	13.3
1.45	0.54	77.1	82	76.8	78.1	77.7	82	13.19
1.13	0.42	77.1	82	76.6	78.1	77.5	82	12.97

DCAT_Calibration_Set1_Test2_20240701.fni (unconverged)

Rad	Gap	Trel	Tmetd	Tawd	Tt	Taws	Tmets	Ps
6.19	0.65	78.2	82	78.1	78.1	78	82	13.56
5.93	0.65	78.1	82	78	78.1	78.1	82	13.55
5.67	0.65	78	82	77.9	78.1	78.1	82	13.55
5	0.65	77.7	82	77.7	78.1	78.1	82	13.54
4.33	0.65	77.5	82	77.5	78.1	78.1	82	13.52
3.76	0.65	77.4	82	77.4	78.1	78.1	82	13.51
3.19	0.65	77.2	82	77.2	78.1	78	82	13.48
2.48	0.65	77.1	82	77.1	78.1	78	82	13.42
1.77	0.65	77.1	82	76.9	78.1	77.8	82	13.3
1.45	0.54	77.1	82	76.8	78.1	77.7	82	13.19
1.13	0.42	77.1	82	76.6	78.1	77.5	82	12.97

DCAT_Calibration_Set1_Test3_20240701.fni (unconverged)

Rad	Gap	Trel	Tmetd	Tawd	Tt	Taws	Tmets	Ps
6.19	0.65	77.6	82	77.6	78.6	78.5	82	13.7

5.93	0.65	77.7	82	77.7	78.6	78.5	82	13.69
5.67	0.65	77.9	82	77.9	78.7	78.6	82	13.69
5	0.65	78	82	78	78.7	78.6	82	13.67
4.33	0.65	78.1	82	78.1	78.7	78.6	82	13.65
3.76	0.65	78.1	82	78.1	78.7	78.6	82	13.64
3.19	0.65	78.1	82	78.1	78.7	78.6	82	13.62
2.48	0.65	78.1	82	78.1	78.7	78.6	82	13.59
1.77	0.65	78.1	82	78.1	78.7	78.6	82	13.54
1.45	0.54	78.1	82	78	78.7	78.5	82	13.51
1.13	0.42	78.1	82	78	78.6	78.5	82	13.45

DCAT_Calibration_Set2_Test1_20240730.fni (unconverged)

Rad	Gap	Trel	Tmetd	Tawd	Tt	Taws	Tmets	Ps
6.19	0.65	83.4	82	83.2	82	82	82	13.35
5.93	0.65	83.2	82	83.1	82.4	82.4	82	13.35
5.67	0.65	83.1	82	83.1	82.7	82.6	82	13.35
5	0.65	82.9	82	82.9	83	83	82	13.34
4.33	0.65	82.8	82	82.8	83.1	83.1	82	13.33
3.76	0.65	82.7	82	82.7	83.1	83.1	82	13.32
3.19	0.65	82.6	82	82.6	83.1	83.1	82	13.31
2.48	0.65	82.6	82	82.6	83.1	83.1	82	13.28
1.77	0.65	82.5	82	82.5	83.1	83	82	13.24
1.45	0.54	82.5	82	82.5	83.1	83	82	13.21
1.13	0.42	82.5	82	82.4	83.1	82.9	82	13.15

DCAT_Calibration_Set2_Test2_20240730.fni

Rad	Gap	Trel	Tmetd	Tawd	Tt	Taws	Tmets	Ps
6.19	0.65	79.60	82.00	79.50	79.70	79.60	82.00	13.57
5.93	0.65	79.60	82.00	79.60	79.80	79.80	82.00	13.57
5.67	0.65	79.60	82.00	79.60	79.90	79.90	82.00	13.56
5.00	0.65	79.60	82.00	79.60	80.10	80.00	82.00	13.55
4.33	0.65	79.60	82.00	79.60	80.20	80.10	82.00	13.53

3.76	0.65	79.60	82.00	79.60	80.20	80.10	82.00	13.52
3.19	0.65	79.60	82.00	79.60	80.20	80.10	82.00	13.50
2.48	0.65	79.50	82.00	79.50	80.20	80.10	82.00	13.47
1.77	0.65	79.50	82.00	79.50	80.10	80.00	82.00	13.42
1.45	0.54	79.50	82.00	79.40	80.10	80.00	82.00	13.38
1.13	0.42	79.50	82.00	79.40	80.10	79.90	82.00	13.32

DCAT_Calibration_Set2_Test3_20240730.fn
i

Rad	Gap	Trel	Tmetd	Tawd	Tt	Taws	Tmets	Ps
6.19	0.65	79.8	82	79.8	81.1	81	82	13.56
5.93	0.65	80.1	82	80.1	81.2	81	82	13.55
5.67	0.65	80.2	82	80.2	81.2	81.1	82	13.54
5	0.65	80.5	82	80.5	81.3	81.2	82	13.52
4.33	0.65	80.6	82	80.6	81.3	81.2	82	13.5
3.76 0.65 80.6 82 80.6 81.3 81.2 82 13.48 3.19 0.65 80.6 82 80.6 81.3 81.2 82 13.46 2.48 0.65 80.6 82 80.5 81.3 81.2 82 13.43 1.77 0.65 80.6 82 80.5 81.3 81.1 82 13.37 1.45 0.54 80.6 82 80.5 81.2 81.1 82 13.33								
1.13	0.42	80.6	82	80.5	81.2	81	82	13.26

Htcd	Vd	Vt	Vs	Htcs	Vrad	Vrc	Qgen
1.32E+01	140.4	65.2	0	1.19E+01	8.37	8.37	0
1.20E+01	134.5	68.1	0	1.23E+01	8.73	8.73	0
1.08E+01	128.6	71	0	1.27E+01	9.14	9.14	0
7.47E+00	113.4	78.7	0	1.37E+01	10.37	10.37	0
3.91E+00	98.2	87.6	0	1.49E+01	11.98	11.98	0
4.36E+00	85.3	97.5	0	1.62E+01	13.81	13.81	0
8.28E+00	72.4	110.6	0	1.79E+01	16.31	16.31	0
1.39E+01	56.3	134.7	0	2.08E+01	21.04	21.04	0
2.11E+01	40.2	176.5	0	2.56E+01	29.68	29.69	0
2.67E+01	32.9	207.9	0	3.04E+01	44.29	44.32	0
3.51E+01	25.6	256.8	0	3.79E+01	73.19	73.34	0

Htcd	Vd	Vt	Vs	Htcs	Vrad	Vrc	Qgen
1.32E+01	140.4	65.2	0	1.19E+01	8.37	8.37	0
1.20E+01	134.5	68.1	0	1.23E+01	8.73	8.73	0
1.08E+01	128.6	71	0	1.27E+01	9.14	9.14	0
7.47E+00	113.4	78.7	0	1.37E+01	10.37	10.37	0
3.91E+00	98.2	87.6	0	1.49E+01	11.98	11.98	0
4.36E+00	85.3	97.5	0	1.62E+01	13.81	13.81	0
8.28E+00	72.4	110.6	0	1.79E+01	16.31	16.31	0
1.39E+01	56.3	134.7	0	2.08E+01	21.04	21.04	0
2.11E+01	40.2	176.5	0	2.56E+01	29.68	29.69	0
2.67E+01	32.9	207.9	0	3.04E+01	44.29	44.32	0
3.51E+01	25.6	256.8	0	3.79E+01	73.19	73.34	0

Htcd	Vd	Vt	Vs	Htcs	Vrad	Vrc	Qgen
5.82E+00	140.4	114.4	0	1.84E+01	1.66	1.66	0
6.08E+00	134.5	107	0	1.75E+01	1.73	1.73	0
6.05E+00	128.6	101.3	0	1.67E+01	1.81	1.81	0

5.11E+00	113.4	91.4	0	1.54E+01	2.06	2.06	0
3.17E+00	98.2	86.1	0	1.47E+01	2.38	2.38	0
5.85E-01	85.3	84.6	0	1.45E+01	2.74	2.74	0
3.49E+00	72.4	85.9	0	1.47E+01	3.23	3.23	0
7.43E+00	56.3	92	0	1.54E+01	4.17	4.17	0
1.19E+01	40.2	106.2	0	1.72E+01	5.86	5.86	0
1.51E+01	32.9	117.6	0	1.95E+01	8.71	8.71	0
1.97E+01	25.6	136.6	0	2.30E+01	14.28	14.28	0

Htcd	Vd	Vt	Vs	Htcs	Vrad	Vrc	Qgen
2.00E+01	162.1	31.1	0	6.52E+00	1.71	1.71	0
1.74E+01	155.2	45.5	0	8.77E+00	1.79	1.79	0
1.53E+01	148.4	55.1	0	1.02E+01	1.87	1.87	0
1.13E+01	130.9	67.4	0	1.19E+01	2.12	2.12	0
8.13E+00	113.4	72	0	1.25E+01	2.45	2.45	0.01
5.33E+00	98.4	74.5	0	1.28E+01	2.83	2.83	0.01
1.76E+00	83.5	77.7	0	1.33E+01	3.34	3.34	0.01
4.82E+00	64.9	85.8	0	1.43E+01	4.3	4.3	0.01
1.02E+01	46.3	102	0	1.63E+01	6.04	6.04	0.01
1.36E+01	38	114.3	0	1.86E+01	8.98	8.98	0.01
1.84E+01	29.6	134	0	2.22E+01	14.72	14.72	0.01

Htcd	Vd	Vt	Vs	Htcs	Vrad	Vrc	Qgen
13.40	162.10	85.10	0.00	14.48	1.68	1.68	0.00
12.25	155.20	86.60	0.00	14.67	1.75	1.75	0.00
11.23	148.40	87.10	0.00	14.73	1.83	1.83	0.00
8.79	130.90	86.10	0.00	14.59	2.08	2.08	0.00
6.24	113.40	84.50	0.00	14.37	2.40	2.40	0.00
3.58	98.40	84.30	0.00	14.32	2.77	2.77	0.00
1.08	83.50	86.20	0.00	14.56	3.27	3.27	0.00

6.18	64.90	93.30	0.00	15.47	4.22	4.22	0.00
11.33	46.30	108.80	0.00	17.40	5.93	5.93	0.00
14.73	38.00	120.90	0.00	19.70	8.81	8.81	0.00
19.51	29.60	140.80	0.00	23.38	14.45	14.46	0.00

Htcd	Vd	Vt	Vs	Htcs	Vrad	Vrc	Qgen
6.83E+00	162.1	129.7	0	2.01E+01	1.68	1.68	0
7.23E+00	155.2	120.4	0	1.89E+01	1.75	1.75	0
7.27E+00	148.4	113.3	0	1.81E+01	1.84	1.84	0
6.36E+00	130.9	101.3	0	1.65E+01	2.09	2.09	0
4.42E+00	113.4	94.7	0	1.57E+01	2.41	2.41	0
1.79E+00	98.4	92.4	0	1.53E+01	2.78	2.78	0
2.67E+00	83.5	93.2	0	1.54E+01	3.29	3.29	0
7.16E+00	64.9	99.5	0	1.62E+01	4.24	4.24	0
1.21E+01	46.3	114.5	0	1.80E+01	5.96	5.96	0
1.54E+01	38	126.6	0	2.03E+01	8.86	8.86	0
2.02E+01	29.6	146.7	0	2.40E+01	14.54	14.54	0

Appendix B

Expt. No.	c_w (purge)	Rotor speed	Pressure				Temperature			Mass Flow Rate			Swirl
			Ambient	Mainstream	Purge Inlet	Hub exit	Mainstream	Purge Inlet	Hub exit	Mainstream	Purge Inlet	Hub exit	
	-	[rpm]	[psia]	[psig]	[psig]	[psig]	[°F]	[°F]	[°F]	[cfm]	[lbm/s]	[lbm/s]	[ft/s]
P-04-001	1602	2600	14.272	14.08	13.68	13.61	76.46	78.98	79.88	1900	0.01313	0.00276	28.22
P-04-002	4005	2600	14.098	13.90	13.63	13.36	76.28	78.08	79.16	1900	0.03277	0.00657	70.87
P-04-003	6569	2600	14.185	13.99	13.92	13.30	76.28	78.62	78.98	1900	0.05380	0.01077	116.14
P-05-001	1923	3000	14.156	13.96	13.58	13.48	81.50	82.04	84.38	1900	0.01583	0.00277	34.12
P-05-002	4806	3000	14.156	13.96	13.73	13.38	78.08	79.70	80.24	1900	0.03942	0.00789	84.97
P-05-003	7370	3000	14.127	13.93	13.94	13.19	78.44	81.14	81.86	1900	0.06058	0.01226	130.25
P-05-004	1923	3000	14.141	13.90	13.42	13.33	75.56	78.98	79.52	2100	0.01576	0.00316	34.12
P-05-005	4806	3000	14.156	13.92	13.60	13.24	80.42	81.50	83.84	2100	0.03953	0.00793	84.97
P-05-006	7370	3000	14.098	13.86	13.78	13.07	80.06	80.96	81.14	2100	0.06057	0.01224	130.25
P-05-007	2083	3400	14.127	13.89	13.40	13.29	79.34	80.60	84.74	2100	0.01711	0.00344	36.75
P-05-008	4806	3400	14.156	13.91	13.59	13.22	80.42	81.50	83.12	2100	0.03953	0.00792	84.97
P-05-009	8171	3400	14.098	13.86	13.88	13.07	81.50	81.50	84.92	2100	0.06720	0.01351	144.36

Notes: The report provides flow rates in scfm, however, the non-dimensional flow rate was used to determine the mass flow rates for the purge inlet and hub exit. Secondly, the mainstream pressure provided is the main air inlet as reported by ASU, however depending on how the model's pressure outlet is defined, a different measurement may be considered